PERGAMON

International Journal of Solids and Structures 37 (2000) 6297–6319

INTERNATIONAL JOURNAL OF SOLIDS and STRUCTURES

www.elsevier.com/locate/ijsolstr

Asymptotic fields for dynamic crack growth in pressure-sensitive elastic–plastic materials

Xi Zhang, Yiu-Wing Mai*

Department of Mechanical and Mechatronic Engineering J07, Centre for Advanced Materials Technology (CAMT), The University of Sydney, Sydney, NSW 2006, Australia

Received 28 January 1999; in revised form 30 August 1999

Abstract

Asymptotic analyses for dynamic propagation of mode I planar cracks in pressure-sensitive elastic–plastic materials have been carried out. The material model adopted is based on the Drucker–Prager yield surface obeying the associate flow rule with linear isotropic hardening. The asymptotic solution is assumed to be of the variable-separable form with a power singularity in the radial coordinate from the crack tip. Attention is focused on the inertia effect on some features of the asymptotic solutions. It is found that for plane-strain cases, the range of pressure sensitivity can be expanded by increasing the crack speed due to a delay in the occurrence of a hydrostatic stress state ahead of the crack tip. An increase in crack speed produces a corresponding change in the characteristics of the governing equations because of a tendency to produce strain and stress 'jumps'. Material and loading mode-dependent speed limits have also been studied under plane-strain and plane-stress conditions. In addition, numerical results are presented for the strength of singularity, the angular distributions of stresses and velocities, and the crack-tip constraint.

Keywords: Asymptotic analysis; Crack-tip plasticity; Pressure sensitivity; Crack dynamics; Strength of singularity

1. Introduction

Since their yielding surfaces are dependent on the mean stress, extension of the classical plasticity theory to include plastic dilatation has a significant consequence for many materials, such as metals, polymers, ceramics and rocks. For example, the void nucleation, growth and coalescence

* Corresponding author. Tel.: +61-2-9351-2290; fax: +61-2-9351-3760.
E-mail address: mai@mech.eng.usyd.edu.au (Y.-W. Mai).

0020-7683/00/$ - see front matter
PII: S0020-7683(99)00276-0

in ductile metals can produce local plastic dilatation so that stress relaxation can happen around the crack tip. A continuum model developed by Gurson (1977) has been often used to investigate the states of stress and strain ahead of the crack tip instead of the classical Prandt–Reuss theory. It successfully captures many features at a later stage of material failure, such as reduction in local stress and enhancement of plastic dilatation. Also, the phase transformation of second-phase particles in ceramics and ceramic composites has aroused much interest in recent years because of the specific mechanism of plastic deformation. (See, for example, Budiansky et al., 1983; Duan et al., 1992 among others). A transformation from *tetragonal to monoclinic* phase of ZrO_2 particles in zirconia-based ceramics and composites can cause a large plastic dilatation with a comparable magnitude of shear strains. Although different failure micro-mechanisms exist in different materials, a useful and appropriate model for the macroscopic material behavior is found to be the Drucker–Prager yield surface with associate flow rule when small deformation is concerned. For instance, the experimental observation of Chen and Reyes-Morel (1986) indicated that the dilatancy is in good agreement with the prediction of the flow rule.

Asymptotic study of near-tip fields, e.g., the singular HRR fields (Hutchinson, 1968; Rice and Rosengen, 1968), plays an important role in establishing useful fracture criteria. In particular, simple cases of quasi-static crack growth in elastic–perfectly plastic materials were analyzed by Slepyan (1974) and Gao (1987). "Quasi-static" is used hereafter in the sense that the inertia effect is negligible. Extension to include plastic reloading on the crack flanks in materials with linear hardening was studied by Ponte-Castaneda (1987) to improve the analyses of Amazigo and Hutchinson (1977) for quasi-static cracks, and were studied by Achenbach et al. (1981) and Ostlund and Gudmumdson (1988) for dynamic cracks. Stahle (1993) considered analytically dynamic crack growth in very low strain-hardening materials, and suggested that inertia might have a significant influence on the fracture process even at fairly low crack tip speeds.

Li and Pan (1990) first studied stationary cracks in pressure-sensitive elastic–plastic materials under plane-strain conditions. Later, Bigoni and Radi (1993) provided useful insight into the asymptotic fields for quasi-static planar cracks in pressure-sensitive materials. Their numerical results indicate that the singularity of stress field decreases with increasing pressure-sensitivity factor and that there is a singular behavior of the yield locus in plane strain.

It is clear from the above that previous studies of asymptotic fields have not considered dynamic crack growth in pressure-sensitive materials. Gao and Nemat-Nasser (1983) and Leighton et al. (1987) have highlighted the effects of inertia on fracture mechanisms. But the quasi-static asymptotic results always leave us with some confusion caused by the ignorance of inertia effects. For plane stress mode-I dynamic cracks, Hermann and Potthast (1995) did provide some insightful information on dynamic crack growth in elastic–plastic materials; but many important issues were left out. For example, the stress and strain discontinuities and the change in the range of pressure-sensitivity arisen from the inertia effect were not considered. Even though they used the plastic wave speed as the limit speed to avoid the effect of fast propagation, it is known that the crack speed could reach as high as the Rayleigh speed in plane stress. So, some salient features were also not studied in their paper. These include the deviation of the maximum opening stress from the crack line and a tendency to produce strain discontinuity or 'jump' at high crack speeds.

The aim of this study is to address the influences of crack velocity on the near-tip fields and on the crack-tip constraint that is defined as the ratio of mean stress to effective stress. This definition adopted here is different from Du and Hancock (1991) and O'Dowd and Shih (1991), but is physically more meaningful and in line with the earlier work of Rice and Tracey (1969) on void growth in rigid plastic solids.

2. Basic equations

2.1. Constitutive relations

Following the works of Drucker and Prager (1953) for granular media, Drucker (1973) for metals and Chen and Reyes-Morel (1986) for ceramics, a simple isotropic elastoplastic model with linear hardening is adopted. The yield locus f in stress space is the combination of two stress invariants,

$$f(\sigma_{ij}) = \tau_e + \mu\sigma_m = H(W^p) \tag{1}$$

where $\tau_e = (s_{ij}s_{ij}/2)^{1/2}$, $s_{ij} = \sigma_{ij} - \sigma_m\delta_{ij}$, $\sigma_m = \sigma_{kk}/3$, W^p is the plastic work, and μ is the pressure-sensitivity factor.

According to the procedure of Li and Pan (1990), the generalized effective stress σ_{ge} which is reduced to non-zero stress components in uniaxial tension, is:

$$\sigma_{ge} = \sigma_e + \sqrt{3}\mu\sigma_m \tag{2}$$

where $\sigma_e = \sqrt{3}\tau_e$.

The value of μ can be obtained from the compressive yield strength σ_c and the tensile yield strength σ_t via the relation given by Needleman and Rice (1978):

$$\mu = \sqrt{3}\frac{\sigma_c - \sigma_t}{\sigma_c + \sigma_t} \tag{3}$$

The experimental data in Carapellici and Yee (1986) showed that the factor μ for glassy bisphenol A-polycarbonate is about 0.14. For ZrO_2-containing ceramics, it may be as high as 0.69 or more, see Chen and Reyes-Morel (1986). It should be noted that this model is reduced to the J_2-flow theory when the parameter μ becomes zero.

It is assumed that the plastic strain follows the associate flow rule. The resultant incremental elastoplastic stress–strain relation between the stress rate $\dot{\boldsymbol{\sigma}}$ and the velocity of deformation $\dot{\varepsilon}$ is:

$$\dot{\varepsilon} = \frac{1}{E}\left[(1+\nu)\dot{\sigma} - \nu\,\mathrm{tr}(\dot{\sigma})\mathbf{I} + \frac{1}{h}\langle\mathbf{Q}\cdot\dot{\sigma}\rangle\mathbf{Q}\right] \tag{4}$$

where ν is the Poisson ratio, E the elastic modulus; h the hardening modulus divided by E, its value can be obtained from the bilinear strain-hardening model as shown in Fig. 1, via the expression, $1/[2(1+\nu)h] = (1/\alpha) - 1$, in which $\alpha = G_t/G$. The symbol $\langle\ \rangle$ denotes the McAulay brackets and $\mathbf{Q}$ is the gradient of the yield surface in stress space,

$$Q_{ij} = \frac{\mu}{3}\delta_{ij} + \frac{\sqrt{3}}{2}\frac{s_{ij}}{\sigma_e} \tag{5}$$

2.2. Kinematics conditions

A Cartesian reference system is shown in Fig. 2 with the origin located at the moving crack tip. For convenience, the polar system is also given. All field variables are referred to the moving Cartesian coordinates (x_1, x_2, x_3) or the cylindrical coordinates (r, θ, x_3). As stated in Ostlund and Gudmumdson (1988), the following identity which relates the material derivative to the spatial derivative along x_1, is well approximated at $r \to 0$:

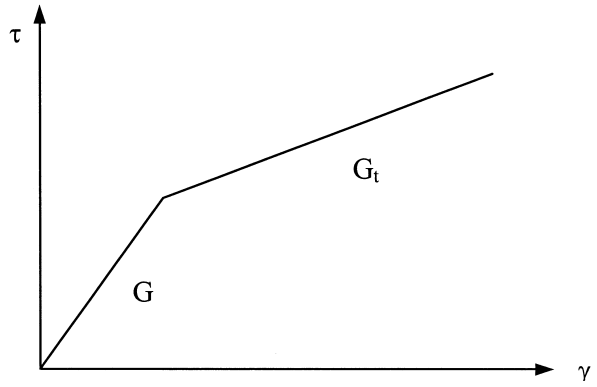

Fig. 1. Shear stress–strain curve in simple shear test.

$$(\cdot) = -V(\,)_{,1} = -V\left[\cos\theta(\,)_{,r} - \frac{\sin\theta}{r}(\,)_{,\theta}\right] \tag{6}$$

where V denotes the crack-tip velocity.

The relations between strain rates and deformation velocities can be written as:

$$\dot{\varepsilon}_{ij} = \frac{1}{2}(v_{i,j} + v_{j,i}) \tag{7}$$

where v_i are the two non-zero in-plane velocities and $v_3 = 0$ for plane-strain cases.

2.3. Equations of equilibrium

Referring to the cylindrical system, under generalized plane stress, the equations of equilibrium take the forms:

$$(r\sigma_{rr})_{,r} + \sigma_{r\theta,\theta} - \sigma_{\theta\theta} = \rho r\dot{v}_r$$

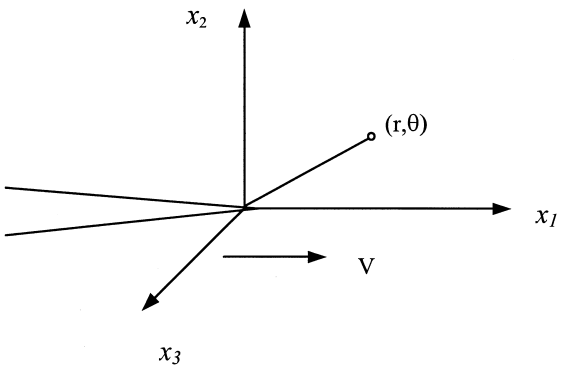

Fig. 2. The reference systems: Cartesian coordinates (x_1, x_2, x_3) and cylindrical coordinates (r, θ, x_3) are centered at the crack-tip and move as the crack grows.

$$(r\sigma_{r\theta})_{,r}+\sigma_{\theta\theta,\,\theta}+\sigma_{r\theta}=\rho r\dot{v}_{\theta} \tag{8}$$

where ρ is the material density and the superposed dot denotes the material time derivatives. The following discussions are based on a relative crack speed, $m_{\mathrm{v}}=V/C_{\mathrm{s}}$, $C_{\mathrm{s}}=\sqrt{G/\rho}$ is the shear wave speed.

2.4. Stress- and strain-rate tensors

Observing the polar coordinate's base vector $\mathbf{e}_r$, $\mathbf{e}_\theta$, we have:

$$\dot{\mathbf{e}}_r=\frac{V}{r}\mathbf{e}_\theta\sin\theta$$

$$\dot{\mathbf{e}}_\theta=-\frac{V}{r}\mathbf{e}_r\sin\theta \tag{9}$$

And the material derivatives of the field variables have the forms:

$$(\dot{\mathbf{e}}_i\mathbf{v})=\dot{\mathbf{e}}_i\mathbf{v}+\mathbf{e}_i\dot{\mathbf{v}}$$

$$\left(\mathbf{e}_i\dot{\sigma}\mathbf{e}_j\right)=\dot{\mathbf{e}}_i\sigma\mathbf{e}_j+\mathbf{e}_i\dot{\sigma}\mathbf{e}_j+\mathbf{e}_i\sigma\dot{\mathbf{e}}_j \tag{10}$$

This yields the following expressions for velocity and stress-rate tensors in the cylindrical coordinates:

$$\dot{v}_r=V\left[\frac{\sin\theta}{r}(v_{r,\,\theta}+v_\theta)-v_r\cos\theta\right]$$

$$\dot{v}_\theta=V\left[\frac{\sin\theta}{r}(v_{\theta,\,\theta}-v_{\theta r})-v_\theta\cos\theta\right] \tag{11}$$

and

$$\dot{\sigma}_{r\theta}=V\left[\frac{\sin\theta}{r}(\sigma_{r\theta,\,\theta}-\sigma_{rr}+\sigma_{\theta\theta})-\sigma_{r\theta,\,r}\cos\theta\right]$$

$$\dot{\sigma}_{rr}=V\left[\frac{\sin\theta}{r}\left(\sigma_{rr,\,\theta}-2\sigma_{r\theta}\right)-\sigma_{rr,\,r}\cos\theta\right]$$

$$\dot{\sigma}_{\theta\theta}=V\left[\frac{\sin\theta}{r}(\sigma_{\theta\theta,\,\theta}+\sigma_{r\theta})-\sigma_{\theta\theta,\,r}\cos\theta\right]$$

$$\dot{\sigma}_{33}=V\left[\frac{\sin\theta}{r}\sigma_{33,\,\theta}-\sigma_{33,\,r}\cos\theta\right] \tag{12}$$

Moreover, Eq. (7) becomes:

$$\dot{\varepsilon}_{rr}=v_{r,\,r}$$

$$\dot{\varepsilon}_{\theta\theta} = \frac{1}{r}(v_{\theta,\,\theta} + v_r)$$

$$\dot{\varepsilon}_{r\theta} = \frac{1}{2}\left[v_{\theta,\,r} + \frac{1}{r}(v_{r,\,\theta} - v_\theta)\right]$$

$$\dot{\varepsilon}_{33} = \begin{cases} 0 & \text{plane strain} \\ v_{3,\,3} & \text{plane stress} \end{cases} \tag{13}$$

2.5. Asymptotic expressions

Linearly strain-hardening plasticity is assumed here, so that the variable-separable asymptotic method holds since all basic equations are elliptic and homogeneous in r. Similar to the procedure of Amazigo and Hutchinson (1977) and Ponte-Castaneda (1987), we have:

$$v_r = \kappa(V/E)r^s/sy_1(\theta)$$

$$v_\theta = \kappa(V/E)r^s/sy_2(\theta)$$

$$\sigma_{r\theta} = \kappa r^s y_3(\theta)$$

$$\sigma_{rr} = \kappa r^s y_4(\theta)$$

$$\sigma_{\theta\theta} = \kappa r^s y_5(\theta)$$

$$\sigma_{33} = \begin{cases} \kappa r^s y_6(\theta) & \text{plane strain} \\ 0 & \text{plane stress} \end{cases} \tag{14}$$

where s is a negative constant, referred to as the singularity index of the near-tip fields, κ is the plastic stress intensity factor (PSIF), which cannot be determined from the asymptotic method; $y_i(\theta)$ are undetermined functions.

2.6. Unloading condition

The critical condition for a material element ahead of the crack tip experiencing elastic unloading depends on the sign of the following plastic multiple. Thus, elastic unloading occurs when:

$$Q_{ij}\dot{\sigma}_{ij} \leq 0 \tag{15}$$

2.7. Reloading conditions

Plastic reloading near the crack flanks has been allowed for in the asymptotic analysis of Ponte-Castaneda (1987) and Bigoni and Radi (1993). The possibility of the existence of a plastic reloading sector has been analyzed when the stress states of a material element in the crack wake reach the yield surface that is left behind after unloading. For pressure-sensitive materials, the critical conditions for

occurrence of plastic reloading are:

$$Q_{ij}\dot{\sigma}_{ij} > 0 \quad \text{and} \quad \frac{\sigma_{ge}(\theta_2)}{\sin^s\theta_2} = \frac{\sigma_{ge}(\theta_1)}{\sin^s\theta_1} \tag{16}$$

where the angles θ_1 and θ_2 correspond to the angles of elastic unloading and plastic reloading, respectively.

2.8. Continuity conditions across the elastic–plastic boundary

It has been proved that for quasi-static crack growth in elastic–plastic materials which are stable in Drucker's sense, the continuities of stress and velocity are satisfied across the elastic–plastic boundary, see Narasimhan and Rosakis (1987). However, as mentioned in Section 1, the continuity is questionable in the presence of inertia effect because discontinuity in strain fields is detected in finite element analyses, such as performed by Varias and Shih (1994). To obtain fully continuous solutions, compete continuities of stresses and velocities are assumed to be valid everywhere and across the elastic–plastic boundary. Thus:

$$\|\sigma_{ij}\| = \|v_i\| = 0 \tag{17}$$

where $\|\ \|$ denotes a 'jump' of the quantity across the boundary.

2.9. Final ODEs

Substituting Eq. (14) into Eqs. (4), (8) and (11)–(13), we can obtain the final governing equations for the crack problems proposed. Its general form can be expressed by:

$$\mathbf{A}\cdot\left\{\frac{\mathrm{d}\mathbf{Y}}{\mathrm{d}\theta}\right\} = \mathbf{B} \tag{18}$$

where matrices **A** and **B** are functions of material parameters and crack-tip velocity. The special forms of these two matrices under plane-strain and plane-stress conditions are given in Appendix A.

2.10. Boundary conditions

Mode I symmetry and the regularity of functions y_i at $\theta = 0$ requires that:

$$y_1'(0) = y_2(0) = y_3(0) = y_4'(0) = y_5'(0) = y_6'(0) = 0 \tag{19}$$

while on the crack surface, tractions $\sigma_{\theta\theta}$ and $\sigma_{r\theta}$ both vanish. Hence:

$$y_3(\pi) = y_5(\pi) = 0 \tag{20}$$

Continuity of all fields requires no 'jump' across the elastic–plastic boundary. Thus:

$$\|y_i\| = 0 \tag{21}$$

Furthermore, the normalization condition must be introduced so that all initial values of y_i are specified at $\theta = 0$, Thus:

$$y_5(0) = 1 \tag{22}$$

Table 1
Numerical results of s, $y_4(0)$, θ_1 and θ_2 under plane-strain condition ($\alpha = 0.75$)

μ	m_v	s	$y_4(0)$	θ_1	θ_2
0	0.0	−0.48066	1.11846	91.58	
	0.6	−0.46849	1.49188	101.59	
	0.8	−0.48993	4.17712	37.31	84.38
0.1	0.0	−0.47539	1.09951	89.03	
	0.6	−0.46228	1.44184	99.74	
	0.8	−0.49049	4.21098	39.28	84.08
0.3	0.0	−0.46318	1.05348	84.84	
	0.6	−0.44806	1.33878	96.46	
	0.8	−0.49116	4.31046	42.70	83.53
0.5	0.0	−0.44983	1.00900	81.67	
	0.6	−0.43250	1.23813	93.48	
	0.8	−0.48980	4.46147	45.70	82.99

2.11. Solution methods

The above system of first-order ordinary differential equations can be solved using standard Runge–Kutta method and Newton–Raphson iteration scheme, as discussed by Press et al. (1992). The values of s and $y_4(0)$ are assigned tentatively. Then, integration is performed and the values of $y_3(\pi)$ and $y_5(\pi)$ are checked. On the basis of the errors in $y_3(\pi)$ and $y_5(\pi)$, new values of s and $y_4(0)$ are assigned by the line search and back-tracking method. The numerical results reported here have been obtained by using a double-precision program with a relative error in each step less than 10^{-8}–10^{-10}. Since the matrix $\mathbf{A}$ in Eq. (18) is singular at $\theta = 0$, a restriction condition $y_4'(\theta) = y_6'(\theta) = 0$ is imposed for the very small angle range ($\theta < 10^{-7}$).

3. Plane strain

3.1. Stress singularity and angular sectors

Tables 1–4 provide the numerical results of s, $y_4(0)$, θ_1 and θ_2 for mode I plane-strain cracks at various crack speeds and material parameters. All results are presented for $\nu = 1/3$. The magnitudes of s at $m_v = 0$ match exactly with the quasi-static results of Bigoni and Radi (1993). As in the case of the J_2-flow theory, $|s|$ is large for high hardening materials and is close to zero for very low hardening materials (i.e. $\alpha \to 0$). In addition, at the same crack speed, the singularity of the fields decreases with increasing μ as reported in Bigoni and Radi (1993). With increasing crack velocity, $|s|$ tends to decrease until a limit velocity is attained. This speed limit $m_v^{\max}$ depends very much on the material constants, for instance, $m_v^{\max} \cong 0.8$ at $\alpha = 0.75$ and $m_v^{\max} \cong 0.1$ at $\alpha = 0.01$. It is noted that the speed limit at $\mu = 0$ is very similar to that predicted by Ostlund and Gudmumdson (1988) in which the crack speed is normalized by the longitudinal wave speed. It is interesting that the speed limit is not strongly affected by μ for all α. Note that the stress singularity approaches -0.5 for $\alpha = 0.75$ if the crack speed is above the limit velocity. This conclusion is consistent with the numerical study of Freund and Douglas (1982) who show that the elastic response dominates the plastic response near the elastic wave speed. However, for low strain hardening materials, this trend has not been found because the speed limit is far lower than the elastic shear wave speed.

Table 2
Numerical results of s, $y_4(0)$, θ_1 and θ_2 under plane-strain condition ($\alpha = 0.1$)

μ	m_v	s	$y_4(0)$	θ_1	θ_2
0	0.0	−0.20957	1.09033	122.21	175.31
	0.2	−0.18137	1.09242	115.43	177.19
	0.3	−0.10924	1.07362	101.36	179.95
0.1	0.0	−0.20179	1.01200	107.60	179.88
	0.2	−0.17743	1.02667	102.65	179.98
	0.3	−0.11179	1.04441	95.94	
0.12	0.2	−0.176864	1.00083	100.80	179.99
	0.3	−0.114332	1.02827	94.96	
	0.31	−0.088937	1.03856	94.62	
0.14	0.3	−0.116347	1.00329	94.16	

Besides the reduction in s, inertia effect also extends the range of μ, as shown in Tables 2 and 4. For quasi-static plane-strain crack growth in pressure sensitive materials, the state of stress on the crack line tends to a hydrostatic tension (i.e., $y_4(0) = 1$) with increasing μ. This also happens for non-zero crack speeds, as given in Tables 1–4 in which $y_4(0) \rightarrow 1$ for some crack speeds. The value of the maximum pressure sensitivity factor μ_{lim} in Bigoni and Radi (1993) is 0.1 for $\alpha = 0.1$ and 0.33 for $\alpha = 0.001$. However, it can be increased to 0.14 for $\alpha = 0.1$ and 0.43 for $\alpha = 0.001$ at their speed limits. It can be seen from Tables 2 and 4 that the occurrence of the hydrostatic tension can be delayed by the inertia effect.

Another influence of material inertia is the change in the characteristics of the governing equations, which is the cause for the speed limit. Based on the coefficients of the system of ODEs listed in Appendix A, the following equations can be obtained for the angular functions of stress rates $\dot{\tilde{\sigma}}_{ij} = \dot{\sigma}_{ij}/(EVr^{s-1})$:

$$\dot{\tilde{\sigma}}_{r\theta} = -b_1 + a_{11}y_1'/2$$

Table 3
Numerical results of s, $y_4(0)$, θ_1 and θ_2 under plane-strain condition ($\alpha = 0.01$)

μ	m_v	s	$y_4(0)$	θ_1	θ_2
0	0.000	−0.08242	0.79744	135.20	146.29
	0.050	−0.07190	0.79613	133.85	147.93
	0.090	−0.04134	0.79661	126.87	156.11
0.1	0.000	−0.07839	0.88495	131.60	144.66
	0.050	−0.06872	0.88148	130.27	146.36
	0.075	−0.05471	0.87735	127.75	149.78
	0.100	−0.01165	0.89747	95.00	179.47
0.2	0.000	−0.07416	0.99042	127.75	143.82
	0.050	−0.06578	0.97773	126.49	145.51
	0.075	−0.05323	0.96304	123.96	148.96
	0.100	−0.01738	0.93746	99.57	174.33

$$\dot{\tilde{\sigma}}_{\theta\theta} = -b_2 + a_{22}y_2' \tag{23}$$

and

$$\dot{\tilde{\sigma}}_{rr} = c_4 - c_{41}a_{11}y_1'/2 - c_{42}a_{22}y_2'$$

$$\dot{\tilde{\sigma}}_{33} = c_6 - c_{61}a_{11}y_1'/2 - c_{62}a_{22}y_2' \tag{24}$$

where c_4 and c_6 are continuous function of θ. $c_{41} = (\alpha_{43}a_{66} - a_{46}a_{63})/D_1$, $c_{42} = (a_{45}a_{66} - a_{46}a_{65})/D_1$, $c_{61} = (a_{63}a_{44} - a_{64}a_{65})/D_1$ and $c_{62} = (a_{65}a_{44} - a_{64}a_{45})/D_1$, and $D_1 = a_{44}a_{66} - a_{64}a_{46}$.

Substituting Eqs. (23) and (24) into Eq. (18), the governing equations for the velocities become:

$$d_{11}y_1'/2 + d_{12}y_2' = e_1$$

$$d_{21}y_1'/2 + d_{22}y_2' = e_2 \tag{25}$$

where e_1 and e_2 are continuous functions of θ, $d_{11} = a_{31} + a_{11}(a_{33} - c_{41}a_{34} - c_{61}a_{36})$, $d_{12} = a_{22}(-c_{42}a_{34} - c_{62}a_{36} + a_{35})$, $d_{21} = a_{11}(-c_{41}a_{54} - c_{61}a_{56} + a_{53})$, and $d_{22} = a_{52} + a_{22}(a_{55} - c_{42}a_{54} - c_{62}a_{56})$.

We denote the determinant of the coefficient matrix in Eq. (25) by $D_2 = d_{11}d_{22} - d_{12}d_{21}$. It can be seen from Fig. 3 that when m_v approaches 0.1, D_2 is equal to zero at $\theta = 90^\circ$. And this would yield the result for y_1' or $y_2' \to \infty$. As a consequence, the rapid variation in velocities can lead to a strain discontinuity. The strain discontinuity caused by non-zero crack speed has been reported in the finite element results of Lam and Freund (1985) and Varias and Shih (1994) from classical elastic–plastic theory. It is also shown that for steady-state crack growth ($m_v = 0$), D_2 is unity everywhere and the strain discontinuity cannot occur in this case. This is consistent with the theoretical analysis of Narasimhan and Rosakis (1987) for quasi-static crack growth in elastic–plastic materials.

The angular positions of elastic unloading θ_1 and plastic reloading θ_2 are also given in Tables 1–4. Clearly, the range of elastic unloading sectors ($\theta_2 - \theta_1$) expands as crack speed increases, except $\alpha =$

Table 4
Numerical results of s, $y_4(0)$, θ_1 and θ_2 under plane-strain condition ($\alpha = 0.001$)

μ	m_v	s	$y_4(0)$	θ_1	θ_2
0.0	0.000	−0.05641	0.75381	137.02	138.52
	0.020	−0.03977	0.74385	136.09	138.62
0.1	0.000	−0.05369	0.82810	133.88	135.56
	0.020	−0.03837	0.81480	132.96	135.81
0.2	0.000	−0.05003	0.89696	130.63	132.56
	0.020	−0.03647	0.88006	129.70	133.13
0.3	0.000	−0.04561	0.96364	127.12	129.75
	0.020	−0.03412	0.94060	126.23	130.57
	0.030	−0.01544	0.90559	123.60	135.20
0.35	0.020	−0.03281	0.97139	124.46	129.46
	0.030	−0.01570	0.93128	121.83	134.25
0.39	0.025	−0.02552	0.97797	122.26	129.80
	0.030	−0.01590	0.95129	120.38	133.57
0.43	0.030	−0.01616	0.97142	118.87	132.98

0.75. The angular range of the elastic unloading zone for low hardening materials also increases with the pressure sensitivity factor.

3.2. Stress components

Fig. 4 shows the angular stress distributions for different crack velocities in the case of $\alpha = 0.01$ and $\mu = 0.1$. Clearly, the difference is very small except the curves at the highest crack velocity $m_v = 0.1$. As in Bigoni and Radi (1993), there is a steep variation in σ_{rr} near the crack flank, as shown in Fig. 4(b), which may contribute to the residual stresses in the crack wake. Its effect on the fracture toughness enhancement is of interest in failure assessment, see Budiansky et al. (1983) and Leighton et al. (1987). At high crack speeds, the extension in the angular range of large normal stresses is evident in Fig. 4. More importantly, the rapid variation of the shear stress $\sigma_{r\theta}$ near $\theta = \pi/2$ is displayed in Fig. 4(a). This tendency to a stress 'jump' may be attributed to the loss of ellipticity of the governing equations as the determinant of coefficient matrix $D_2 \rightarrow 0$ in Fig. 3. It is interesting to note that the location for strain discontinuity is the same as the numerical results in Lam and Freund (1985) and Varias and Shih (1994).

The angular variations of hydrostatic and effective stresses with crack speed for $\alpha = 0.01$ and $\mu = 0.1$ are given in Fig. 5. The extensions of the angular regions with high mean stress and low effective stress for $m_v = 0.1$ are clearly shown in this figure.

3.3. Crack-tip constraint

The non-uniqueness of hydrostatic stress ahead of the crack tip under different specimen geometry has been rigorously studied in the past, see, for example, Matsoukas et al. (1986), Wu et al. (1995) and Hancock et al. (1993). Thus, usage of the fracture toughness measured with small-size laboratory specimens for failure assessment of large-size engineering structures is often invalid. The crack-tip

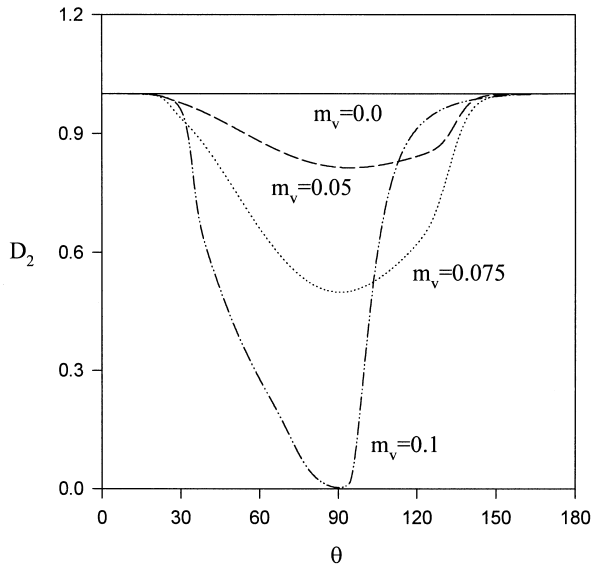

Fig. 3. Typical plots of the angular variations of D_2 obtained for various crack speeds for the cases of $\alpha = 0.01$ and $\mu = 0.1$ in plane strain.

constraint can be quantified in terms of T-stress as in Du and Hancock (1991) or Q*-stress as in O'Dowd and Shih (1991). Considering the importance of mean and effective stresses in the failure criteria for cleavage fracture and ductile tearing, and in the evolution equations of micro defects, like voids and shear bands, it seems reasonable to define the crack tip constraint as the ratio of mean stress to effective stress. Thus:

$$\frac{\sigma_{\mathrm{m}}^{\mathrm{total}}}{\sigma_{\mathrm{e}}} = \frac{\sigma_{\mathrm{m}}^{\mathrm{singular}}}{\sigma_{\mathrm{e}}} + \frac{Q^*/f(T)}{\sigma_{\mathrm{e}}} \tag{26}$$

Fig. 6 shows the angular distributions of the first term in the RHS of Eq. (26) at different crack speed and pressure-sensitive factor. It is shown that a near constant value is obtained for $\sigma_{\mathrm{m}}/\sigma_{\mathrm{e}}$ ahead of the crack tip and the angular range with constant stress ratio increases with crack velocity. But increasing crack speed has little influence on its magnitude when m_v is less than 0.075. At high crack speeds, $m_v \geq 0.075$, however, the increasing trend in the stress ratio is detectable from Fig. 6(a). In addition, an increase in μ reduces the stress ratio rapidly as shown in Fig. 6(b).

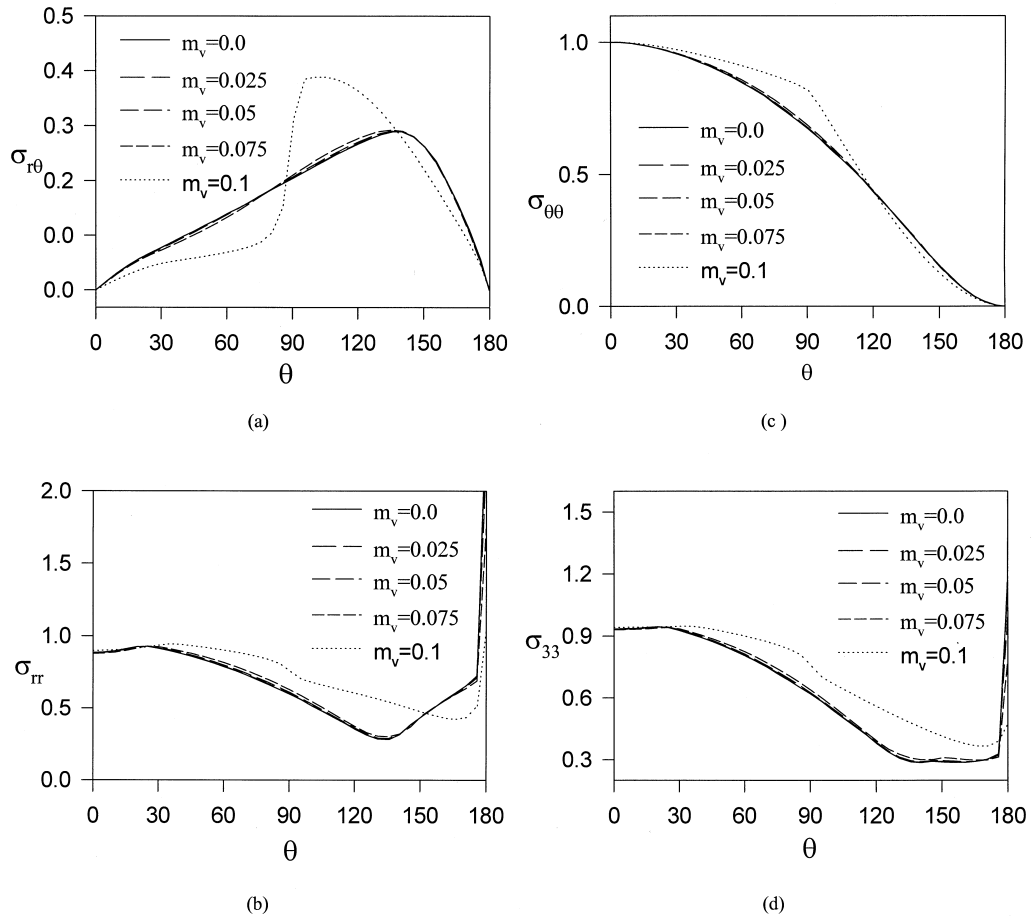

Fig. 4. Angular distributions of four stress components for various crack speeds under the condition $\alpha = 0.01$ and $\mu = 0.1$ in plane strain.

3.4. Velocity fields

Fig. 7 shows the angular distributions of velocities for $\alpha = 0.01$ and $\mu = 0.1$. When the crack speed is large, that is $m_v = 0.1$, there appears to be a kink in v_r at $\theta = 90^\circ$. The assumption of strain discontinuity or 'jump' is, hence, reconfirmed here. This fast variation in velocities can lead to increases in the stresses defined in Eqs. (23) and (24), although the magnitudes are substantially reduced by the coefficients a_{11} and a_{22}. Conversely, it is shown that the plastic strains ahead of the crack tip become small by increasing the crack speed due to reductions in the magnitude of v_r and the gradient of v_θ.

4. Plane stress

4.1. Singularity index and angular sectors

Numerical results for the strength of singularity s, the elastic unloading angle θ_1 under plane-stress

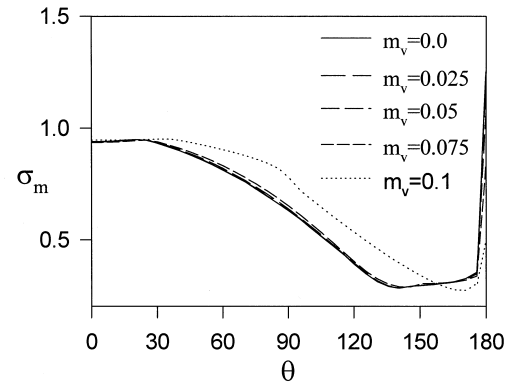

(a)

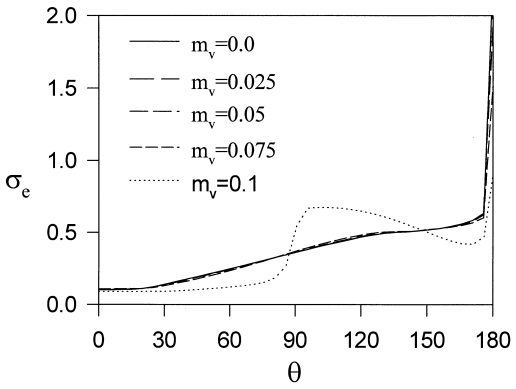

(b)

Fig. 5. Angular distributions of hydrostatic and effective stresses for different crack speeds for the cases of $\alpha = 0.01$ and $\mu = 0.1$ in plane strain.

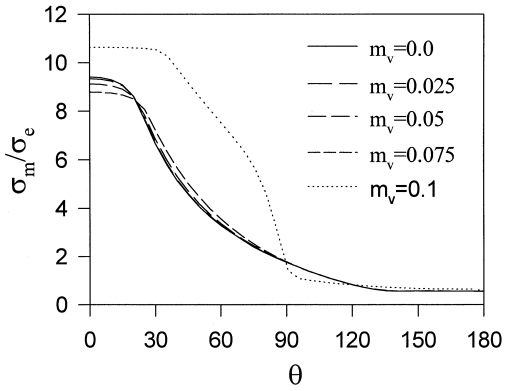

(a)

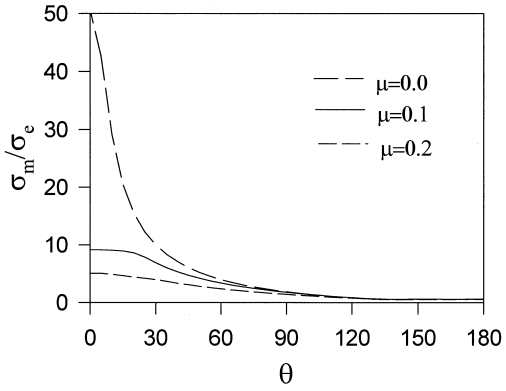

(b)

Fig. 6. Angular distributions of the stress ratio σ_m/σ_e in the case of $\alpha = 0.01$: (a) for different crack speed at $\mu = 0.1$ and (b) for different values of μ at $m_v = 0.05$ in plane strain.

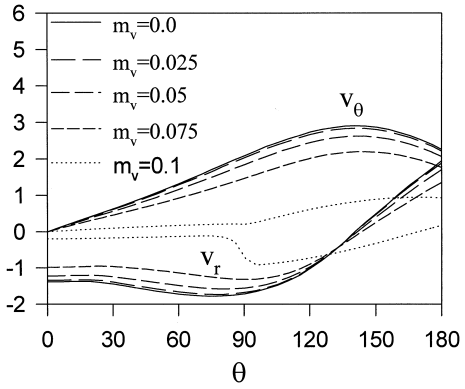

Fig. 7. Angular distributions of velocity fields for different crack speeds in the case of $\alpha = 0.01$ and $\mu = 0.1$ in plane strain.

Table 5
Numerical results of s, $y_4(0)$, θ_1 under plane-stress condition ($\alpha = 0.1$)

μ	m_v	s	$y_4(0)$	θ_1
0	0.00	−0.23725	0.62269	73.89
	0.20	−0.23024	0.63354	75.49
	0.40	−0.19677	0.68629	81.83
	0.60	−0.24727	0.73465	41.21
	0.80	−0.30142	0.88220	36.44
	0.85	−0.19664	1.30524	47.60
0.2	0.00	−0.21812	0.51935	69.61
	0.20	−0.21169	0.53002	71.14
	0.40	−0.18056	0.58575	77.47
	0.60	−0.22020	0.62231	38.45
	0.80	−0.28356	0.74405	31.95
	0.85	−0.19331	1.14560	41.27
0.4	0.00	−0.20382	0.41795	66.17
	0.20	−0.19795	0.42859	67.66
	0.40	−0.16932	0.48594	73.91
	0.60	−0.19871	0.51908	36.36
	0.80	−0.26381	0.62899	29.16
	0.85	−0.23409	0.84901	32.92
0.8	0.00	−0.18500	0.20315	61.32
	0.20	−0.18020	0.21453	62.69
	0.40	−0.15717	0.27429	68.57
	0.60	−0.16996	0.31790	33.63
	0.80	−0.22667	0.42869	25.77
	0.85	−0.23330	0.57342	25.73

Table 6
Numerical results of s, $y_4(0)$, θ_1 under plane-stress condition ($\alpha = 0.01$)

μ	m_v	s	$y_4(0)$	θ_1
0	0.00	−0.08629	0.53024	61.27
	0.20	−0.06549	0.54186	40.09
	0.40	−0.10004	0.52840	22.33
	0.60	−0.13682	0.52726	15.81
	0.80	−0.20113	0.54327	12.47
0.2	0.00	−0.07946	0.42792	56.02
	0.20	−0.05745	0.44052	36.69
	0.40	−0.08575	0.42538	20.16
	0.60	−0.11677	0.42392	14.14
	0.80	−0.17412	0.43839	10.98
0.4	0.00	−0.07475	0.32282	52.20
	0.20	−0.05185	0.33709	34.17
	0.40	−0.07525	0.32029	18.44
	0.60	−0.10223	0.31842	12.80
	0.80	−0.15380	0.33231	9.85
0.8	0.00	−0.06978	0.08236	46.35
	0.20	−0.05003	0.09954	30.97
	0.40	−0.06043	0.08142	16.01
	0.60	−0.08222	0.07796	10.92
	0.80	−0.12505	0.09343	8.30

conditions are presented in Tables 5–7 for $\nu = 0.5$ and $\alpha = 0.001$, 0.01 and 0.1. The magnitudes of s and θ_1 at vanishing crack speeds are consistent with the quasi-static results obtained by Bigoni and Radi (1993) under plane-stress conditions. For the dynamic cases, if we normalize the crack speed by the longitudinal wave speed, we obtain $s = -0.23211$ and $\theta_1 = 74.87^\circ$ for $\alpha = 0.1$ and $m_L = 0.1$ ($m_L = V/C_L$, $C_L = \sqrt{E/\rho}$). This result agrees very well with $s = -0.232$ and $\theta_1 = 74.75^\circ$ as obtained by Ostlund and Gudmumdson (1988). Note that the range of crack speeds and pressure-sensitive factors is much larger than that in plane strain. It can be expected that this is caused by the delay of the occurrence of $D_2 = 0$ and the elimination of the singular behavior of the yield locus. The crack speed can reach as high as the Rayleigh speed regardless of the material's hardening index. But there exists a crack speed limit, $m_v^{\lim}$, below which the stress singularity decreases with increasing crack speed. This limit, $m_v^{\lim}$, decreases with decreasing hardening index. (See Tables 5 and 6.) It vanishes for $\alpha = 0.001$. This phenomenon can only be found at $\alpha = 0.75$ for plane strain, and it cannot be detected for small α. It is interesting that in low strain-hardening materials, the strength of singularity ($-s$) also decreases with crack speed. In contrast, there is a decreasing trend in plane strain as shown in Tables 2–4. In addition, the values of s at high crack speeds can be several times of those for quasi-static growth for $\alpha = 0.001$. Plastic reloading is not considered for plane stress. The angular range of plastic zones increases with crack speed, if it is not very large, for high and medium hardening materials. However, for small α, only the decreasing trend in the plastic sectors is detected and θ_1 decreases rapidly when the crack speed approaches the elastic wave speed. For example, when $\alpha = 0.001$, $\mu = 0.8$ and $m_v = 0.6$, the range of the plastic zone is 0.0622, less than 5°.

Different from the results for plane-strain cases where the elastic response caused by inertia effect can only be dominant at high α's, the inertia effect becomes the main reason for cracks to propagate in a brittle manner even for small α's. It is found from Tables 6 and 7 that the inertia effect can increase the stress singularity and reduce the plastic zone to a narrow strip ahead of the crack tip. Hermann and

Table 7
Numerical results of s, $y_4(0)$, θ_1 under plane-stress condition ($\alpha = 0.001$)

μ	m_v	s	$y_4(0)$	θ_1
0	0.00	−0.02867	0.50788	54.44
	0.20	−0.03280	0.50473	16.02
	0.40	−0.04669	0.50285	8.59
	0.60	−0.06249	0.50267	5.84
	0.80	−0.09606	0.50437	4.42
0.2	0.00	−0.02658	0.40657	49.92
	0.20	−0.02818	0.40359	13.97
	0.40	−0.03991	0.40182	7.35
	0.60	−0.05335	0.40164	4.97
	0.80	−0.08208	0.40312	3.75
0.4	0.00	−0.02516	0.30147	43.55
	0.20	−0.02489	0.29857	12.45
	0.40	−0.03522	0.29682	6.47
	0.60	−0.04707	0.29663	4.35
0.8	0.00	−0.02394	0.05664	36.86
	0.20	−0.02042	0.05389	10.43
	0.40	−0.02904	0.05177	5.32
	0.60	−0.03886	0.05153	3.56

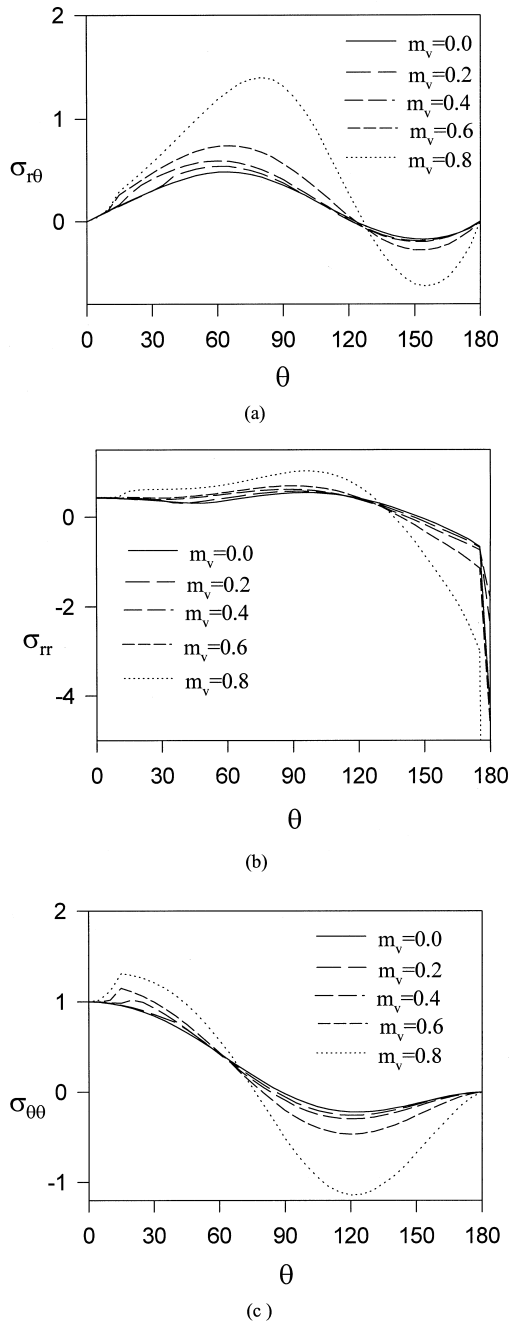

Fig. 8. Angular distributions of three stress components for various crack speeds under the condition $\alpha = 0.01$, $\mu = 0.2$ in plane stress.

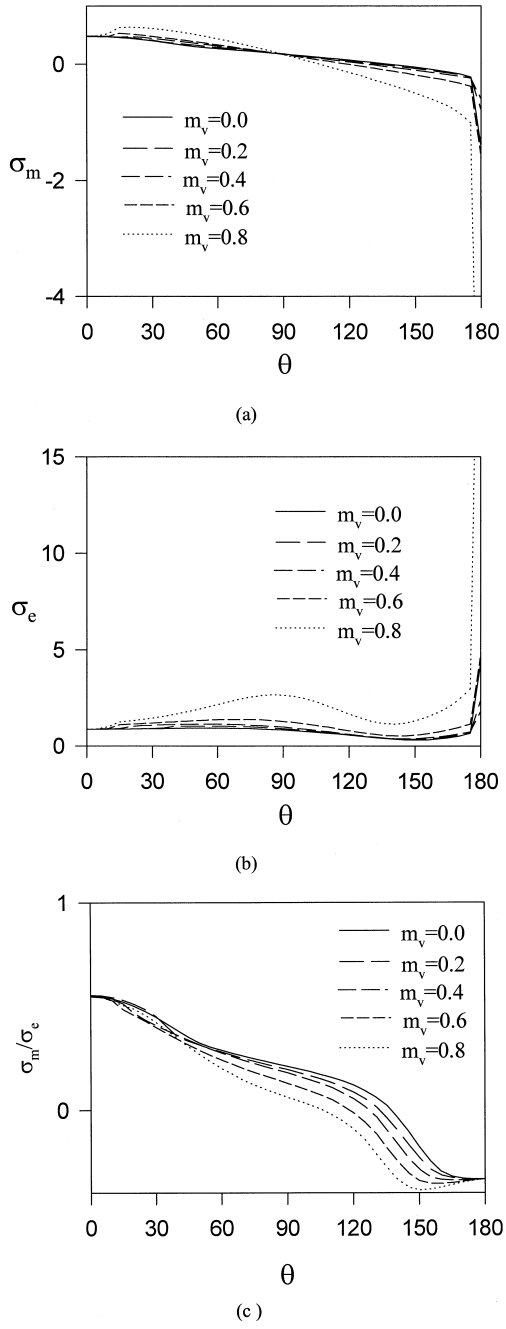

Fig. 9. Angular distributions of (a) hydrostatic stresses, (b) effective stresses and (c) σ_m/σ_e ratio for different crack speeds for the cases of $\alpha = 0.01$ and $\mu = 0.1$ in plane stress.

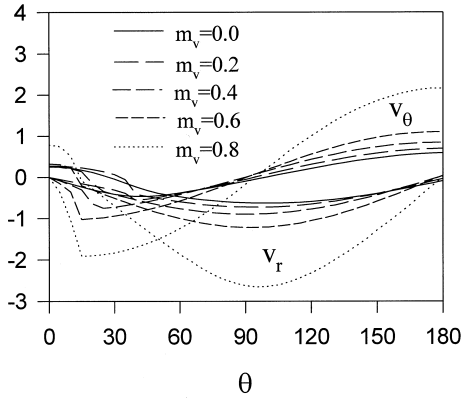

Fig. 10. Angular distributions of velocity fields in the case of $\alpha = 0.01$ for different crack speeds in plane stress.

Potthast (1995) cannot obtain this conclusion in their work because they have restricted the crack speed to lower than the plastic shear wave speed, $C_{\mathrm{spl}} = \sqrt{G_{\mathrm{t}}/\rho}$.

4.2. Stress fields

Fig. 8 shows the variation of stress components with crack speed for $\alpha = 0.01$ and $\mu = 0.2$. An increase in crack velocity causes obvious changes in all stress components. A kink in the $\sigma_{\theta\theta}$ curves is detected. The maximum hoop stress ahead of the crack tip shown in Fig. 8(c) is located in a direction at about 15° to the crack line when $m_v = 0.6$–0.8. It increases with crack speed. This feature was first mentioned by Yoffe (1951) as due to the inertia effect and was used to explain the tendency for a growing crack in brittle materials to bifurcate or to branch. It is concluded that this mechanism also exists in ductile materials, but the deflected angle is much smaller than 60° provided by Yoffe (1951). So, plasticity can confine the crack branches to propagate only slightly away from the crack line. Another feature is the rapid increase in shear stress at $\theta = \pi/2$ when $m_v \geq 0.8$. Relatively low normal stress and large shear stress near $\theta = \pi/2$ may be the driving force for the formation of shock waves when m_v approaches the Rayleigh wave speed.

It can be seen from Fig. 9 that there exists a small variation in angular distributions of the mean and effective stresses ahead of the crack tip with increasing crack speed. The ratio $\sigma_{\mathrm{m}}/\sigma_{\mathrm{e}}$ ahead of the crack tip is not affected much by crack speed. This means that the crack-tip constraint plays a negligible role for failure assessment in plane stress.

4.3. Velocity fields

The angular variations of near-tip velocity fields are plotted in Fig. 10 for different crack speed for cases of $\alpha = 0.01$ and $\mu = 0.2$. It shows a kink, or a tendency to produce a strain 'jump', at the elastic–plastic boundary. This kink becomes more significant when m_v approaches the Rayleigh wave speed. The plastic deformation in the plastic sector becomes intense at high crack speeds although the plastic zone shrinks. Deng and Rosakis (1991) argued that the intense deformation ahead of the crack tip is a good reason to adopt a shear strain failure criterion.

5. Conclusions

Asymptotic analyses have been carried out in this paper for mode I planar dynamic cracks in pressure-sensitive materials with linear hardening. Numerical results are provided to account for the inertia effect. Conclusions similar to quasi-static crack growth studied by Bigoni and Radi (1993) are recovered for a variety of material parameters for cases of zero crack speed. The results reveal many features about the strength of the singularity, the size of active plastic zone and near-tip variations of stress and velocity fields. The following are the most important conclusions of this work.

5.1. Plane strain

1. An increase in crack velocity reduces the stress singularity and the plastic deformation ahead of the crack tip. But there exists a crack speed limit due to the requirement of fully continuous near-tip fields. This speed limit, $m_v^{\max}$, decreases with the material hardening index α, and it is much less than the elastic wave speed at low α. All results are restrained by the condition that the crack speed is below this speed limit.
2. The calculated results indicate that the speed limit is caused by the loss of ellipticity of the governing equations. The kinks in stress and strain fields evidently lead to corresponding discontinuities or 'jumps'. However, Drugan (1998) has excluded the discontinuity for subsonic dynamic crack growth on thermodynamics arguments. The inconsistency of his theoretical study with numerical results, such as obtained by Lam and Freund (1985), Deng and Rosakis (1991) and Varias and Shih (1994), and the asymptotic analyses of Ponte-Castaneda (1987), Ostlund and Gudmumdson (1988) and the present work, begs further studies.
3. The occurrence of the hydrostatic state of stress ahead of the crack tip can be delayed by the inertia effect. Asymptotic solutions can be obtained for high values of m_v and μ. It is seen that the inertia effect becomes more significant at large μ.
4. The constraint effect should be taken into account at high crack speeds when α and μ are large. It is found that the ratio of mean to effective stresses decreases sightly when the crack speed is not too large. But high crack speeds can increase the stress ratio remarkably.

5.2. Plane stress

1. There is no restriction on crack speed provided that it is less than the Rayleigh wave speed. For large or medium strain-hardening indices, the strength of singularity would decrease with increasing crack speed until a speed limit is attained. Beyond this limit, s will increase with crack speed. However, for fast crack growth in low hardening materials, the strength of singularity increases with all crack speeds studied. In contrast, it decreases in all plane-strain cases.
2. The plastic deformation ahead of the crack tip becomes intense with increasing crack speed, though the plastic zone is reduced.
3. There are kinks in the stress and velocity fields at the elastic–plastic boundary. As the crack speed increases, so is the gradient of the angular distributions. It is shown that a change in the characteristics of the governing equations happens when the crack speed approaches the Rayleigh wave speed.
4. Inertia effect cannot change the crack-tip constraint because the stress ratio seems insensitive to the variation of crack speed.

Acknowledgements

The authors would like to express their gratitude to the Australian Research Council (ARC) for the continuing support of this project. X. Zhang acknowledges an Overseas Postgraduate Research Studentship from the Australian Government tenable at the University of Sydney and an ARC Scholarship from the research grant awarded to Y.-W. Mai.

Appendix A. The coefficients of matrices *A* and *B*

The coefficients of the matrices **A** and **B** in Eq. (18) are given below:

$$a_{11} = 2\frac{c_v}{s}\sin^2\theta, \quad a_{13} = -1;$$

$$a_{22} = \frac{c_v}{s}\sin^2\theta, \quad a_{25} = -1;$$

$$a_{31} = -1, \quad a_{33} = s\left(1 + \nu + \frac{2}{h}Q_{r\theta}Q_{r\theta}\right),$$

$$a_{34} = \frac{s}{h}Q_{rr}Q_{r\theta}, \quad a_{35} = \frac{s}{h}Q_{\theta\theta}Q_{r\theta}, \quad a_{36} = \frac{s}{h}Q_{33}Q_{r\theta};$$

$$a_{43} = \frac{2}{h}Q_{r\theta}Q_{rr}, \quad a_{44} = 1 + \frac{1}{h}Q_{rr}Q_{rr}$$

$$a_{45} = -\nu + \frac{1}{h}Q_{\theta\theta}Q_{rr}, \quad a_{46} = -\nu + \frac{1}{h}Q_{33}Q_{rr};$$

$$a_{52} = -1, \quad a_{53} = \frac{2s}{h}Q_{r\theta}Q_{\theta\theta}, \quad a_{54} = s\left(-\nu + \frac{1}{h}Q_{rr}Q_{\theta\theta}\right),$$

$$a_{55} = s\left(1 + \frac{1}{h}Q_{\theta\theta}Q_{\theta\theta}\right), \quad a_{56} = s\left(-\nu + \frac{1}{h}Q_{33}Q_{\theta\theta}\right);$$

$$a_{63} = \frac{2}{h}Q_{r\theta}Q_{33}, \quad a_{64} = -\nu + \frac{1}{h}Q_{rr}Q_{33},$$

$$a_{65} = -\nu + \frac{1}{h}Q_{\theta\theta}Q_{33}, \quad a_{66} = 1 + \frac{1}{h}Q_{33}Q_{33}.$$

$$b_1 = c_v\sin\theta\left(y_1\cos\theta + \frac{\sin\theta}{s}y_2\right) + s(y_3\cos\theta + y_4\sin\theta)$$

$$b_2 = c_v \sin\theta\left(y_2\cos\theta - \frac{\sin\theta}{s}y_1\right) + s(y_5\cos\theta + y_3\sin\theta)$$

$$b_3 = \frac{s-1}{2}y_2$$

$$b_4 = y_1$$

$$b_5 = y_1$$

$$b_6 = 0$$

in which $c_v = m_v^2/[2(1+\nu)]$.

It should be mentioned that any coefficient related to the x_3-direction must be cancelled out in the plane-stress cases.

References

Achenbach, J.D., Kanninien, M.F., Popelar, C.H., 1981. Crack tip fields for fast fracture of an elastic–plastic material. J. Mech. Phys. Solids 29, 211–225.

Amazigo, J., Hutchinson, J.W., 1977. Crack-tip fields in steady crack-growth with linear strain hardening. J. Mech. Phys. Solids 25, 81–97.

Bigoni, D., Radi, E., 1993. Mode I crack propagation in elastic–plastic pressure sensitive materials. Int. J. Solids Structures 30, 899–919.

Budiansky, B., Hutchinson, J.W., Lambropoulos, J.C., 1983. Continuum theory of dilatant transformation toughening in ceramics. Int. J. Solids Structures 19, 337–355.

Carapellici, L.M., Yee, A.F., 1986. The biaxial deformation and yield behavior of bisphenol-A polycarbonate: effect of anisotropy. Polym. Engng. Sci 26, 920–930.

Chen, I.W., Reyes-Morel, P.E., 1986. Implications of transformation plasticity in ZrO_2-containing ceramics. Part I: Shear and dilatation effects. J. Am. Ceram. Soc 69, 181–189.

Deng, X., Rosakis, A.J., 1991. Dynamic crack propagation in elastic–perfectly plastic solids under plane stress conditions. J. Mech. Phys. Solids 39, 683–722.

Drucker, D.C., 1973. Plasticity theory of strength-differential (SD) phenomenon, and volume expansion in metals and plastics. Metall. Trans 4, 667–673.

Drucker, D.C., Prager, W., 1953. Soil mechanics and plastic analysis and limit design. Q. Appl. Math 10, 157–165.

Drugan, W.J., 1998. Thermodynamic equivalence of steady-state shocks and smooth waves in general media; applications to elastic–plastic shocks and dynamic fracture. J. Mech. Phys. Solids 46, 313–336.

Du, Z.Z., Hancock, J.W., 1991. The effect of non-singular stresses on crack-tip constraint. J. Mech. Phys. Solids 39, 557–567.

Duan, K., Cotterell, B., Mai, Y.-W., 1992. Stress intensity factors for ceramics toughened by microcracking caused by dilatant second phase particles. Int. J. Solids Structures 29, 231–242.

Freund, L.B., Douglas, A.S., 1982. The influence of inertia on elastic–plastic antiplane-shear crack growth. J. Mech. Phys. Solids 30, 59–74.

Gao, Y.C., 1987. Plane stress dynamic plastic field near a propagating crack tip. Int. J. Fracture 34, 117–129.

Gao, Y.C., Nemat-Nasser, S., 1983. Dynamic fields near a crack tip growing in elastic–perfectly-plastic solids. Mech. Mater 2, 47–60.

Gurson, A.L., 1977. Continuum theory of ductile rupture by void nucleation and growth. Part I: Yield criteria and flow rules for porous ductile media. J. Engr. Mater. Tech 99, 2–15.

Hancock, J.W., Reuter, W.G., Parks, D.M., 1993. Constraint and toughness parameterized by T. In: Constraint Effects in Fracture, ASTM STP 1171. American Society for Testing and Materials, Philadelphia, pp. 21–40.

Hermann, L.P., Potthast, B., 1995. Asymptotic crack tip fields for pressure-sensitive materials and dynamic crack growth under plane stress conditions. Int. J. Fract 74, R53–R61.

Hutchinson, J.W., 1968. Singular behavior at the end of a tensile crack in hardening material. J. Mech. Phys. Solids 16, 13–31.
Lam, P.S., Freund, L.B., 1985. Analysis of dynamic growth of a tensile crack in an elastic–plastic material. J. Mech. Phys. Solids 33, 153–167.
Leighton, J.T., Chanpion, C.R., Freund, L.B., 1987. Asymptotic analysis of steady dynamic crack growth in elastic–plastic material. J. Mech. Phys. Solids 35, 139–157.
Li, F.Z., Pan, J., 1990. Plane strain crack-tip fields for pressure-sensitive dilatant materials. J. Appl. Mech 57, 40–49.
Matsoukas, G.M., Cotterell, B., Mai, Y.-W., 1986. Hystrostatic stress and crack opening displacement in three-point bend specimen with shallow cracks. J. Mech. Phys. Solids 34, 499–510 See also Erratum: J. Mech. Phys. Solids 35, 1987, 675–676.
Narasimhan, R., Rosakis, A.J., 1987. Re-examination of jumps across quasi-statically propagating surface under generalized plane stress in anisotropically hardening elastic–plastic solids. J. Appl. Mech 54, 519–524.
Needleman, A., Rice, J.R., 1978. Limits to ductility set by plastic flow localization. In: Koisitinien, D.P., Wang, N.M. (Eds.), Mechanics of Sheet Metal Forming. Plenum Press, NY, pp. 237–267.
O'Dowd, P., Shih, C.F., 1991. Family of crack-tip fields characterized by a triaxility parameter. Part I: Structure of fields. J. Mech. Phys. Solids 39, 898–1015.
Ostlund, S., Gudmumdson, P., 1988. Asymptotic crack tip fields for dynamic fracture of linear-hardening solids. Int. J. Solids Structures 24, 1141–1148.
Ponte-Castaneda, P., 1987. Asymptotic fields in steady crack growth in linear strain-hardening. J. Mech. Phys. Solids 35, 227–268.
Press, W.H., Flannery, B.P., Teukolsky, S.A., Vetterling, W.T., 1992. Numerical Recipes. Cambridge University Press, Cambridge, UK.
Rice, J.R., Rosengen, G.T., 1968. Plane strain deformation near a crack tip in a power-law hardening material. J. Mech. Phys. Solids 16, 1–12.
Rice, J.R., Tracey, D.M., 1969. On the ductile enlargement of voids in triaxial stress fields. J. Mech. Phys. Solids 17, 201–217.
Slepyan, L.I., 1974. Growing crack during plane deformation of an elastic–plastic body. Mekhamika Tverdogo Tela 9, 57–67.
Stahle, P., 1993. Dynamic crack tip field at steady growth and vanishing strain-hardening. J. mech. Phys. Solids 41, 919–936.
Varias, A.G., Shih, C.F., 1994. Dynamic steady crack growth in elastic–plastic solids: propagation of strong discontinuity. J. Mech. Phys. Solids 42, 1817–1848.
Wu, S.-X., Mai, Y.-W., Cotterell, B., 1995. Prediction of the initiation of ductile fracture. J. Mech. Phys. Solids 43, 798–810.
Yoffe, E.H., 1951. The moving Griffith crack. Phil. Mag 42, 739–750.